

*Supplement of*

**Machine learning for improvement of upper tropospheric relative humidity in ERA5 weather model data**

- 5 Ziming Wang et al.  
*Correspondence to:* Ziming Wang (Ziming.Wang@dlr.de)

## S1 Evaluation of ERA5 temperature using IAGOS in the UTLS

Simmons et al. (2014) found a temperature uncertainty of 0.1 K near the tropopause in the tropics in the precursor of ERA5 data, the ERA-Interim reanalysis. Figure S1 compares  $T_{IAGOS}$  and  $T_{ERA5}$  for the same test data set used for further ANN model evaluation (10% samples randomly selected from all collected IAGOS waypoints around cruise altitudes between 200 hPa and 400 hPa over the North Atlantic Region (NAR) in 2020). The good agreement between both temperatures is reflected in all tested scenarios - all sky UT, cloudy UTLS, clear sky UTLS, and all sky UT - indicated by high determination coefficients ( $R^2$  of 0.96 - 0.98). The spread of the correlation corresponds to greater variability in  $T_{IAGOS}$  when the aircraft flew through clouds or due to the interpolation of the gridded  $T_{ERA5}$  to the aircraft's vertical position. The MAE between  $T_{IAGOS}$  and  $T_{ERA5}$  varies between 0.72 K and 0.88 K across the entire data sets.  $T_{ERA5}$  has a relatively more obvious cold bias in clear sky UTLS and all sky LS regions, with larger MAE and smaller  $R^2$  values among these four scenarios.

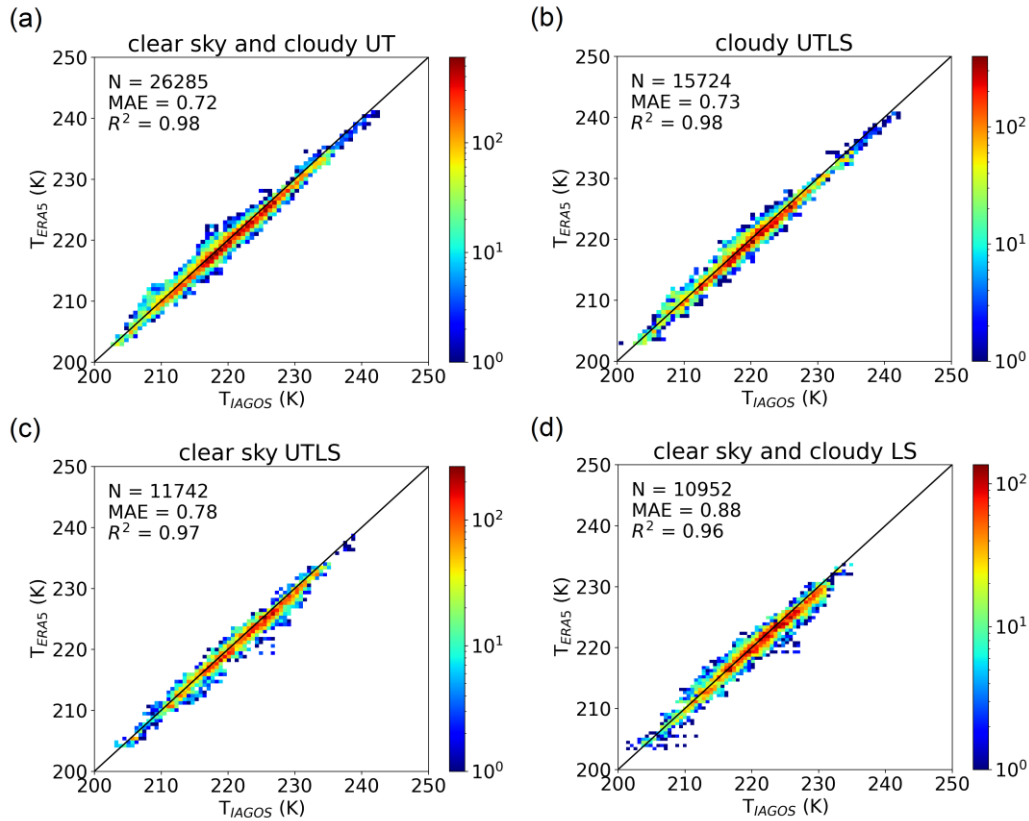
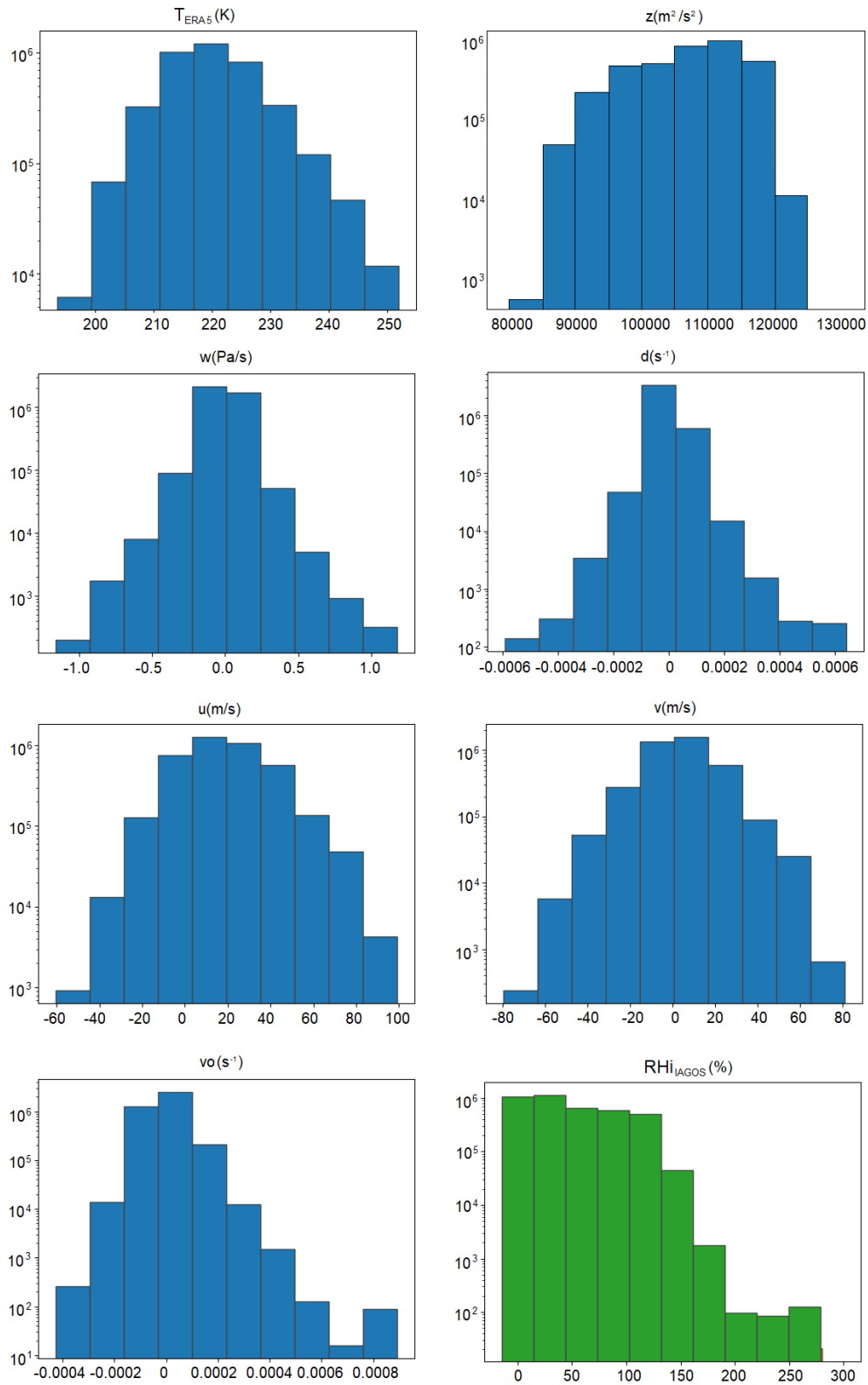


**Figure S1: Comparisons of  $T_{ERA5}$  against  $T_{IAGOS}$  in (a) clear sky and cloudy UT, (b) cloudy UTLS, (c) clear sky UTLS, and (d) clear sky and cloudy LS in the test data set between 200 hPa and 400 hPa over the Atlantic, Europe and Africa for the year 2020.**

## 20 S2 Preparation of training and validation data

Accounting for the typical time spans of water vapor transport mechanisms, including deep convection, warm conveyor belt uplift regimes, and slow ascending flows, the criteria for data combination involve a 2-hour and 6-hour time lag before IAGOS data acquisition,  $\pm 2$  pressure layers from ERA5, and the current humidity measurements from IAGOS. Subsequently, a data set comprising 4 million samples is compiled for training, validation, and testing.

25 To ensure model robustness, 10% of the samples are randomly excluded from the training set to construct an independent test data set. The remaining training sets of the ANN model, with  $RHi_{IAGOS}$  or  $q_{IAGOS}$  as the target output, are further subdivided into an 80% training subset and a 10% evaluation subset, respectively. While the primary focus is on improving predictions of higher RHi values and ice supersaturation, the complete range of RHi values supplied to the neural networks enhances the overall accuracy of the model.



30

**Figure S2: Distributions of input variables including  $T_{ERA5}$  (K),  $z$  ( $m^2/s^2$ ),  $w$  (Pa/s),  $d$  ( $s^{-1}$ ),  $u$  (m/s),  $v$  (m/s), and  $vo$  ( $s^{-1}$ ) from ERA5 and target  $RHi_{IAGOS}$  in the ANN model. The trend of  $RHi_{ERA5}$  for the test dataset (10% randomly selected from all samples) is shown in Fig. 6.**

35

Distributions of the input and target values in the training data sets are sketched in Fig. S2. Notably, they are not uniformly distributed due to the performed selections as well as the usage of different weather conditions. For instance,  $T_{ERA5}$  spans a range from approximately 193 K to 252 K, and the geopotential  $z$  encompasses values between roughly 8000  $m^2/s^2$  and 12500

$\text{m}^2/\text{s}^2$ .  $RHi_{IAGOS}$  values vary across the entire spectrum, ranging from 0 % to 275 %. For the derivation of  $q_{IAGOS}$ , the saturation water vapor pressure over ice,  $p_{ice}$ , is first calculated using the equation in Murphy and Koop (2005),

$$p_{ice} = e^{(9.550426 - 5723.265/T_{IAGOS} + 3.53968 \ln(T_{IAGOS}) - 0.00728332 T_{IAGOS})} \quad (1)$$

An earlier comparison between different parameterizations of  $p_{ice}$  showed that the differences are less than 0.5% for temperatures greater than -173.15 K (Schumann, 2012). In the next step,  $q$  is calculated from RHi according to,

$$q = \frac{RHi \times p_{ice} \times R_0}{p \times R_1} \quad (2)$$

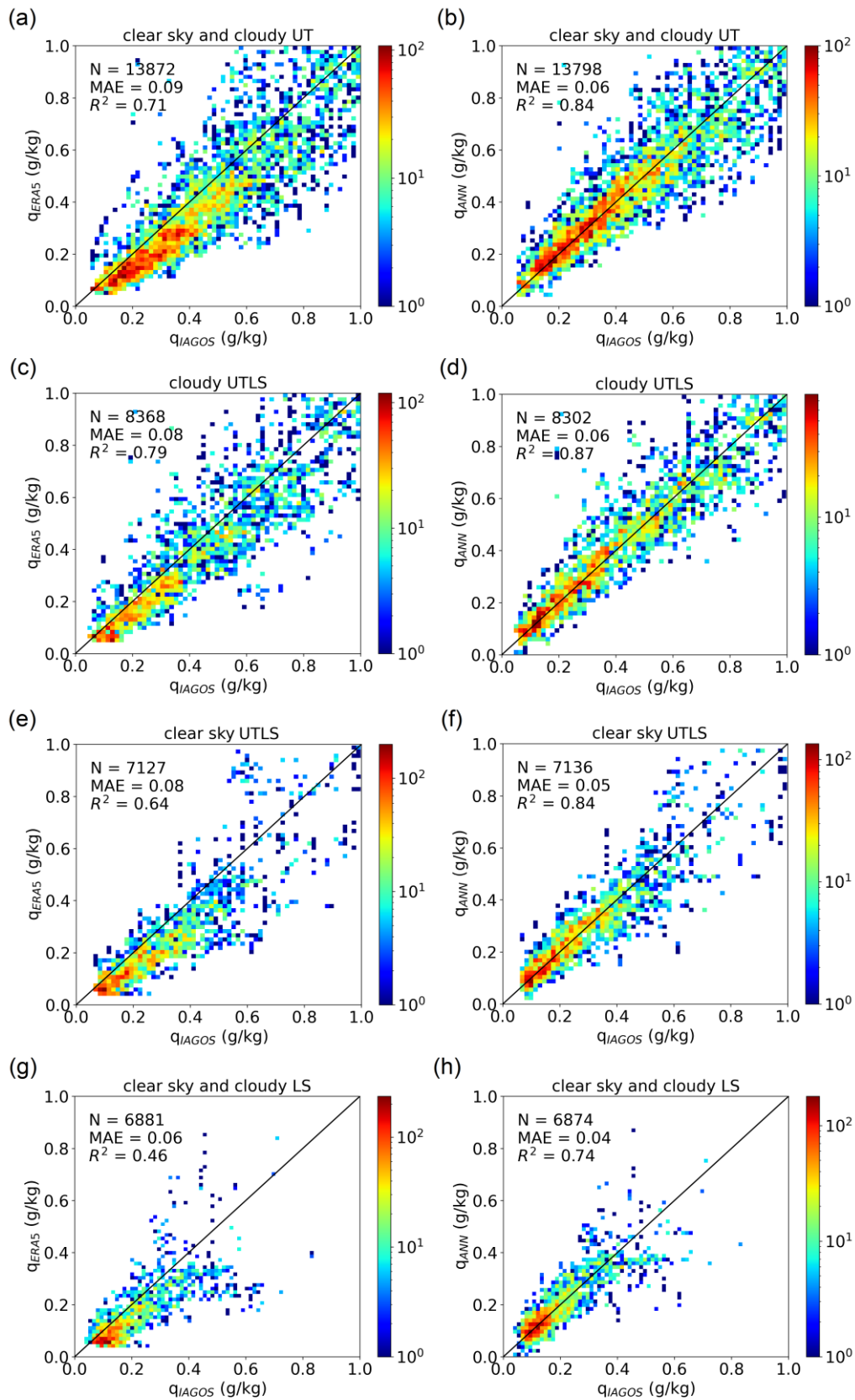
where  $p$  is the pressure altitude (Pa),  $R_0$  (287.05  $\text{Jkg}^{-1}\text{K}^{-1}$ ) and  $R_1$  (461.51  $\text{Jkg}^{-1}\text{K}^{-1}$ ) are the real gas constants for air and water vapor, respectively.

### S3 Validation of ANN specific humidity in clear and cloudy conditions in the ULTS

$q_{ANN}$  exhibit increased correlations with  $q_{IAGOS}$  ( $R^2 \geq 0.74$ ) and decreased bias ( $\text{MAE} \leq 0.06$  g/kg) across all scenarios, as evidenced in Fig. S3, when evaluated on its test dataset. In the all sky UT (cloudy UTLS) areas, the bias is reduced for  $q_{ANN}$  compared to  $q_{ERA5}$ , with an increase of  $R^2$  by 0.13/0.08 and a decrease of MAE by 0.03/0.02 g/kg. In the clear UTLS (all sky LS) regimes, the increase of  $R^2$  is 0.20/0.28, and the decrease of MAE is 0.03/0.02 g/kg).

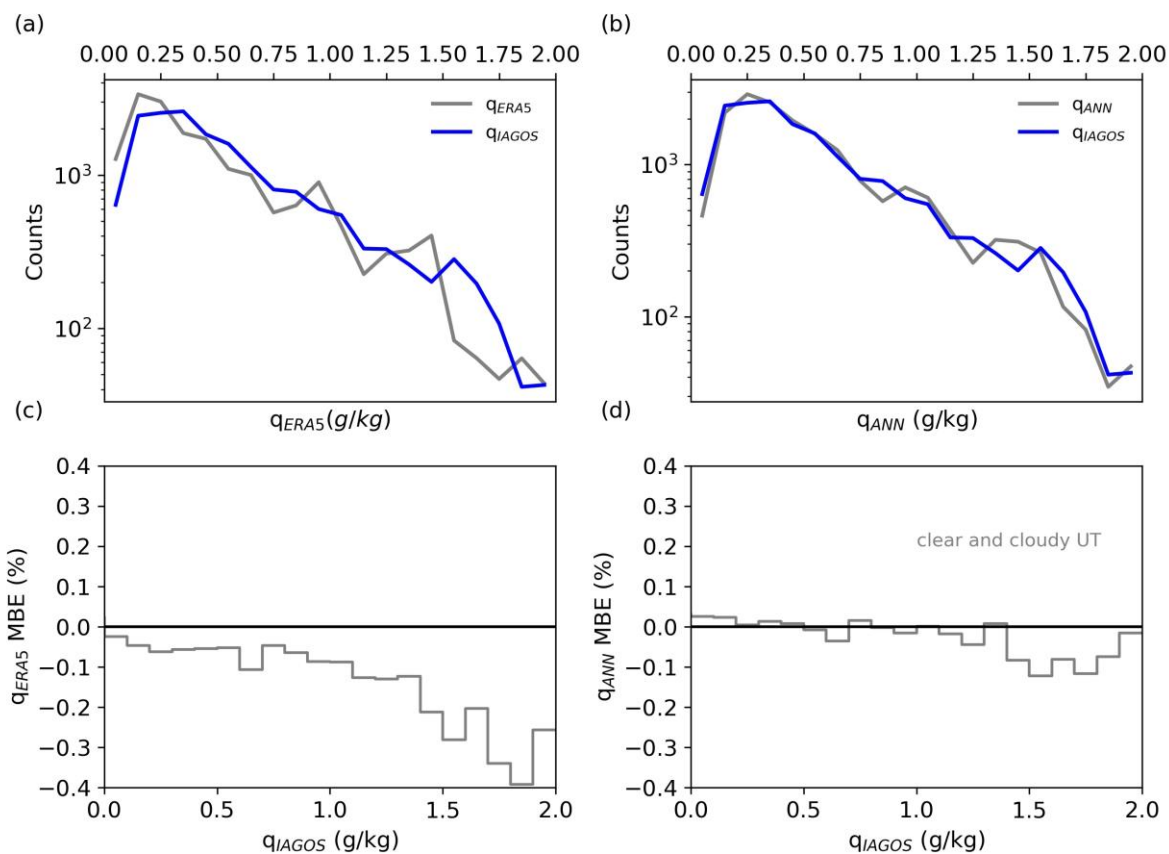
The assessment of specific humidity compared to  $q_{IAGOS}$  reveals a noticeably higher dispersion concerning the results with respect to  $RHi_{ERA5}$  and  $RHi_{ANN}$ . This increased uncertainty can be attributed to biases arising from the transition process between  $RHi_{IAGOS}$  and  $q_{IAGOS}$ . The presence of 'vertical points' in each plot, deviating from the regression line, indicates limited data points and infrequent measurements under extreme conditions. This, in turn, contributes to the abnormal values in these instances.

The consistency between  $q_{ANN}$  and  $q_{IAGOS}$  in Fig. S4b is better than that between  $q_{ERA5}$  and  $q_{IAGOS}$  in Fig. S4a. In Fig. S4c, the MBE of  $q_{ERA5}$  compared with  $q_{IAGOS}$  is always negative, with the bias increasing up to 0.4 g/kg when  $q_{IAGOS}$  reaches 2 g/kg. In Fig. S4d, the ANN model improves the accuracy of  $q$  predictions, showing a minor overestimation for lower water vapor concentrations and an underestimation compared to  $q_{IAGOS}$  that is rarely smaller than that of  $q_{ERA5}$ .



60

**Figure S3: Comparison of  $q_{ERA5}$  (left column) and  $q_{ANN}$  (right column) against  $q_{IAGOS}$  in the (a) and (b) clear sky and cloudy UT, (c) and (d) cloudy UTLS, (e) and (f) clear sky UTLS, and (g) and (h) clear sky and cloudy (or all sky) LS regions in the test data set.**



65 **Figure S4: Frequency distribution (a and c) and overall mean biased error MBE (%) (b and d) of  $q_{ERA5}$  and  $q_{ANN}$  against  $q_{IAGOS}$  in the clear sky and cloudy UT (grey) in the test data set.**

#### S4 Comparisons with independent aircraft measurements

The water vapor measurement from AIMS (Atmospheric Ionization Mass Spectrometer) instrument using a backward heated inlet has been evaluated and shown to be in good agreement with other high-quality water vapor data (Kaufmann et al., 2018). Therefore, in addition to the IAGOS measurements, this study uses the independent humidity data records from AIMS  
70 (Kaufmann et al., 2016) aboard the HALO aircraft in special weather situations during the CIRRU-SHL campaign to validate the accuracy of RH<sub>i</sub> prediction from the ANN model.

On 21 July 2021, HALO departed from Germany in the early morning and detected one strong contrail case over the Iberian Peninsula at cruise level. Figure S5a and c present  $RH_{i,ERA5}$  and  $RH_{i,ANN}$  along the HALO flight track from 06:11 UTC to 09:08 UTC within the pressure levels of 161 to 262 hPa. Compared with AIMS measured  $RH_{i,AIMS}$ , the wet bias of  $RH_{i,ERA5}$   
75 can reach up to 40% (reddish points) in Fig. S5b. In contrast, the ANN model can reduce the RH<sub>i</sub> overestimation in the UTLS region within the range of  $\pm 10\%$  (cyan or green points in Fig. S5d).

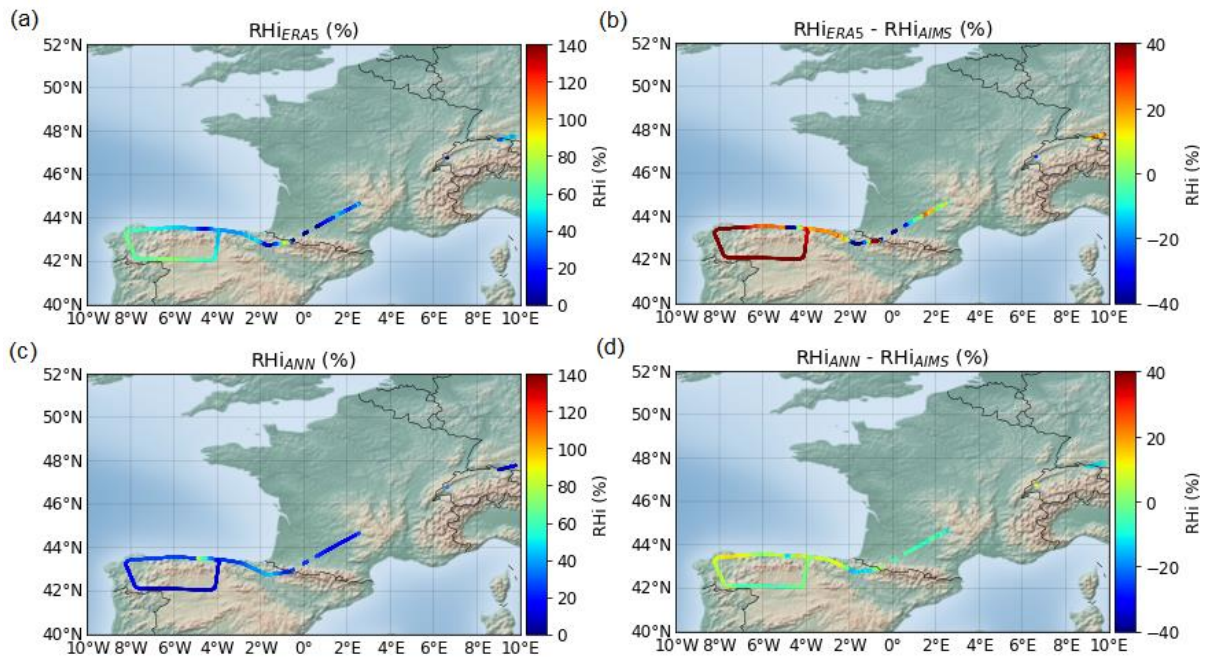


**Figure S5: RHi derived from (a) ERA5 or (c) the ANN model and the differences relative to AIMS measurements in (b) and (d) obtained from the HALO aircraft on 21 July 2021 during the CIRRUS-HL campaign.**

80

### References

Murphy, D. M. and Koop, T.: Review of the vapour pressures of ice and supercooled water for atmospheric applications, *Q. J. Roy. Meteor. Soc.*, 131, 1539–1565, <https://doi.org/10.1256/qj.04.94>, 2005.

Schumann, U.: A contrail cirrus prediction model, *Geosci. Model Dev.*, 5, 543–580, <https://doi.org/10.5194/gmd-5-543-2012>, 2012.

85

Simmons, A. J., Poli, P., Dee, D. P., Berrisford, P., Hersbach, H., Kobayashi, S., and Peubey, C.: Estimating low-frequency variability and trends in atmospheric temperature using ERA-Interim, *Q. J. Roy. Meteor. Soc.*, 140, 329–353, <https://doi.org/10.1002/qj.2317>, 2014.